Physics Letters B 743 (2015) 451–455

Contents lists available at ScienceDirect

Physics Letters B

www.elsevier.com/locate/physletb

# Neutron-driven collectivity in light tin isotopes: Proton inelastic scattering from $^{104}$Sn

A. Corsi [a,*], S. Boissinot [a], A. Obertelli [a], P. Doornenbal [b], M. Dupuis [c], F. Lechaftois [c], M. Matsushita [d], S. Péru [c], S. Takeuchi [b], H. Wang [b,e], N. Aoi [f], H. Baba [b], P. Bednarczyk [g], M. Ciemala [g,n], A. Gillibert [a], T. Isobe [b], A. Jungclaus [h], V. Lapoux [a], J. Lee [b], M. Martini [m], K. Matsui [i], T. Motobayashi [b], D. Nishimura [j], S. Ota [d], E. Pollacco [a], H. Sakurai [b,i], C. Santamaria [a], Y. Shiga [k], D. Sohler [l], D. Steppenbeck [d], R. Taniuchi [i]

[a] CEA, Centre de Saclay, IRFU/Service de Physique Nucléaire, F-91191 Gif-sur-Yvette, France
[b] RIKEN Nishina Center, 2-1 Hirosawa, Wako, Saitama 351-0198, Japan
[c] CEA/DAM/DIF, 91297 Arpajon, France
[d] CNS, The University of Tokyo, RIKEN Campus, Wako, Saitama 351-0198, Japan
[e] State Key Laboratory, Peking University, Beijing, PR China
[f] RCNP Osaka University, Ibaraki, Osaka 567-0047, Japan
[g] The Niewodniczanski Institute of Nuclear Physics, Krakow, Poland
[h] Instituto de Estructura de la Materia, CSIC, E-28006 Madrid, Spain
[i] Department of Physics, University of Tokyo, Bunkyo, Tokyo 113-0033, Japan
[j] Department of Physics, Tokyo University of Science, Noda, Chiba 278-8510, Japan
[k] Department of Physics, Rikkyo University, Toshima, Tokyo 172-8501, Japan
[l] Institute for Nuclear Research, Debrecen, Hungary
[m] Department of Physics and Astronomy, Ghent University, Proeftuinstraat 86, B-9000, Gent, Belgium
[n] Grand Accélérateur National d'Ions Lourds (GANIL), CEA/DSM-CNRS/IN2P3, F-14076 Caen Cedex 5, France

ARTICLE INFO

*Article history:*
Received 23 October 2014
Received in revised form 10 February 2015
Accepted 9 March 2015
Available online 12 March 2015
Editor: V. Metag

*Keywords:*
Collectivity
Inelastic scattering
Gamma spectroscopy

ABSTRACT

Inelastic scattering cross sections to individual bound excited states of $^{104}$Sn were measured at 150 MeV/u beam energy and analyzed to evaluate the contribution of neutron and proton collectivity. State-of-the-art Quasi-Particle Random Phase Approximation (QRPA) with the D1M Gogny interaction reproduces the experimental proton collectivity and our inelastic scattering cross sections once used as input for a reaction calculation together with the Jeukenne–Lejeune–Mahaux (JLM) potentials. Experimental inelastic scattering cross section decreases by 40(24)% from $^{112}$Sn to $^{104}$Sn. The present work shows that (i) proton and neutron collectivities are proportional over a large range of tin isotopes (including $^{104}$Sn), as is typical for isoscalar excitations, and (ii) the neutron collectivity dominates. It suggests that the plateau in the mass range A = 106–112 displayed by E2 transition probabilities is driven by neutron collectivity.



The evolution of nuclear shell structure along isotopic or isotonic chains has revealed unexpected onsets of collectivity or shell gap modifications [1–3]. The proton-closed shell Sn isotopes form an ideal testing ground to study the evolution of shell structure and collectivity with isospin. Experimental results reported in [4,5] provide a signature of the magicity of $^{100}$Sn and $^{132}$Sn. According to the seniority scheme, the reduced transition probabilities B(E2; $0_1^+ \rightarrow 2_1^+$) (B(E2) in the following) in Sn isotopes are expected to exhibit a parabolic trend with a maximum at mid-shell. The experimental trend instead is asymmetric with a persistence of proton collectivity approaching the doubly magic $^{100}$Sn [6–11]. Three Coulomb excitation experiments have been reported recently [12–14] for $^{104}$Sn, the most neutron-deficient isotope for which the $0_1^+ \rightarrow 2_1^+$ transition probability has been accessed to date. While [12] claims a drop of the experimental B(E2) in agreement with large-scale shell model calculations, the authors of [13,14] have measured a smoother decrease at N = 54. Up to now, no shell model calculation can explain satisfactorily the tins' B(E2)

* Corresponding author.
*E-mail address:* acorsi@cea.fr (A. Corsi).

http://dx.doi.org/10.1016/j.physletb.2015.03.018

systematics [6–9,12–14]. Calculations systematically underestimate collectivity from $^{112}$Sn down to $^{104}$Sn. Truncations applied to the valence space used to run shell model calculations are pointed out as responsible for the missing collectivity in $^{104-106}$Sn [13–15] and no clear microscopic understanding has been achieved yet.

Beyond-mean field approaches, which do not suffer from valence space restrictions, have been also applied to tin isotopes [16–19]. Different calculations using the QRPA approach find an increase of collectivity going from the mid-shell towards the lightest tin until $^{106,108}$Sn. The QRPA approach was compared to a Generator-Coordinate-Method-based model using the same mean field [19]. The former is found to be more suitable to describe the spectroscopy of rather spherical nuclei such as semi-magic tin isotopes.

No information is available on neutron collectivity in light tin isotopes. The neutron transition matrix element $M_n$ can be estimated from proton inelastic scattering cross sections provided the proton transition matrix element $M_p(L) = \sqrt{B(EL)/(2L+1)}$ is known [20–22].

Inelastic scattering experiments have been performed only for stable tin isotopes ($^{112}$Sn–$^{124}$Sn) [20,23]. We report here on the first measurement of inelastic scattering on hydrogen for a neutron deficient tin, namely $^{104}$Sn.

The experiment was performed at the Radioactive Isotope Beam Factory operated by the RIKEN Nishina Center and the Center for Nuclear Study (CNS) of the University of Tokyo. The $^{104}$Sn beam at 150 MeV/u was produced with an intensity of 350 pps via fragmentation of a $^{124}$Xe primary beam at 6 pnA on a 0.555 g.cm$^{-2}$ $^{9}$Be target and separated via the BigRIPS separator [24]. A measurement with a $^{112}$Sn beam at 170 MeV/u was performed as a reference. The beam impinged on a $CH_2$ (C) target of 192.1 (370.5) mg.cm$^{-2}$. The cross section on hydrogen was extracted by subtracting from the $CH_2$ spectrum the one measured on carbon, after normalization. The setup consisted of the DALI2 array composed of 186 NaI scintillators [25] for gamma-ray detection and the ZeroDegree Spectrometer for downstream particle identification [26]. A mass resolution of $\sigma \sim 0.001$ was achieved, allowing for an unambiguous isotopic identification. A total of $1.5 \times 10^7$ and $1.7 \times 10^7$ $^{104}$Sn ions was identified at the ZeroDegree focal plane during the measurement with $CH_2$ and C targets, respectively. The scintillators of the DALI2 array were calibrated in energy with $^{137}$Cs, $^{88}$Y and $^{60}$Co sources, with gamma emission ranging between ∼600 and ∼1800 keV. The efficiency of the DALI2 array, covering angles between 19 and 150 degrees, was 14% at 1.33 MeV. This value was in relative agreement within 6% with the Geant4 simulation [27] and was rather independent of the angular distribution of the emitted gamma radiation thanks to the large solid angle coverage. The FWHM intrinsic energy resolution evaluated from Cs, Co and Y sources scaled as $2.4\sqrt{E}$, consistently with [25]. The gamma spectra of $^{104}$Sn ($^{112}$Sn) inelastically scattered on C and $CH_2$ targets were Doppler corrected with $\beta = 0.47$ and 0.45 (0.495 and 0.485), respectively.

The gamma spectrum of $^{112}$Sn shown in Fig. 1 displays a transition at 1245(15) keV and a broad structure around 800–1100 keV. This structure was found in coincidence with the 1245 keV transition as shown in the inset of Fig. 1. Since the spectroscopy of $^{112}$Sn is well known [28], we considered three transitions in this peak: 930(30), 985(30) and 1090(30) keV, corresponding to the $0_2^+ \to 2_1^+$, $4_1^+ \to 2_1^+$ and $3_1^- \to 2_1^+$ transitions, respectively.

In order to extract the cross section to the excited states observed in this experiment, the spectrum was adjusted with the sum of a double-exponential background and the simulated response function of the DALI2 array to the gamma-transitions mentioned above. The background originated mainly from atomic processes (bremsstrahlung in the target) at low energy ($E_\gamma < 500$ keV),

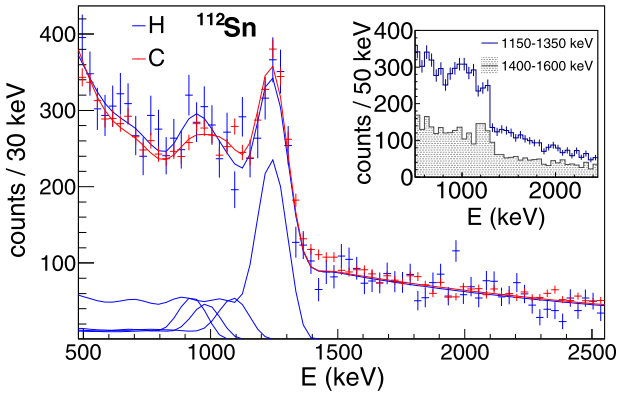


**Fig. 1.** (Color online.) Gamma spectra of $^{112}$Sn inelastically scattered on C (red) and H (blue). The solid line is the fit function used to extract the cross sections (sum and contributions from each transition, for H only). The inset shows the gated gamma spectra ($CH_2$ + C) of $^{112}$Sn in coincidence with the $2_1^+ \to 0_1^+$ transition and with an adjacent gamma energy window.

from Compton scattering and target breakup at higher gamma energy. We could not extract the angular distribution of the observed transition, due to the limited statistics. We quantified the effect of the uncertainty on the angular distribution through simulations. The photo peak efficiency for a 1 MeV transition emitted isotropically in the center of mass at $\beta \sim 0.5$ was 24%, whereas the same transition emitted with an anisotropic angular distribution as the one shown in [25] leads to a detection efficiency of 22%. This was considered in the error bars of the inclusive cross sections. The adjustment procedure was performed using spectra with and without addback between adjacent crystals of DALI2 array, yielding consistent results. If a state was both directly excited and populated by the feeding from higher-lying states, as happens here for $2_1^+$, the feeding was subtracted in order to obtain the direct population cross section. The error on the cross section was obtained as the sum of the error issued from the $\chi^2$ minimization (which includes statistical error), the uncertainty on DALI2 efficiency (6% relative systematic error), the statistical error on the number of incident beam particles, and a 2% uncertainty on target thickness. Note that for overlapping peaks (as in the case of the structure observed in $^{112}$Sn at energy between 800 and 1100 keV, see Fig. 1) the adjustment procedure was affected by a large uncertainty whereas the sum of the cross sections to the states feeding the $2^+$ state was reliable.

As a cross check, the cross section on H was also obtained as the difference of the cross sections on $CH_2$ and C, namely $\sigma_H = (\sigma_{CH_2} - \sigma_C)/2$, where $\sigma_{CH_2}$ is the effective cross section per atom of the target. Results were found consistent with the ones obtained on the H spectrum.

We finally obtained cross sections on H of 9.1(38), 3.6(26), 4.0(24) and 4.6(20) mb for the $2_1^+$, $4_1^+$, $0_2^+$ and $3_1^-$ states, respectively. The cross sections on C target for the same states were found to be 22.5(35), 5.9(32), 4.7(29) and 12.3(27) mb.

In the $^{104}$Sn spectrum shown in Fig. 2 (up), four transitions are visible at 670(20), 1040(20), 1260(15) and 1950(50) keV. The transitions at 670(20) and 1260(15) keV are in good agreement with the known energy of $4_1^+ \to 2_1^+$ decay at 682 keV and $2_1^+$ state [28]. The 1260 keV transition was found in coincidence with the three other ones, which therefore correspond to the decay of feeders to the $2_1^+$ state (Fig. 2, bottom). Prompt transitions are consistent only with E1, M1, E2 multipolarities. Since the final state is a $2_1^+$, the initial state spin must be J = 0 to 4 for angular momentum conservation. Inelastic scattering measurements on nuclei with few neutrons outside the closed shell show that the $3_1^-$ state is strongly populated. The inelastic scattering cross section to the $3_1^-$ state of

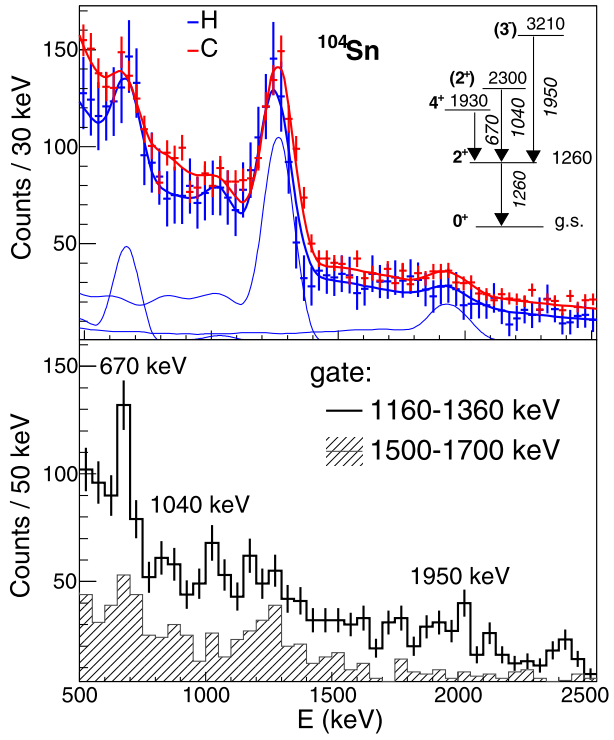


**Fig. 2.** (Color online.) Top: gamma spectra of $^{104}$Sn inelastically scattered on C (red) and H (blue). The solid line is the fit function used to extract the cross sections (sum and contributions from each transition, for H only). Bottom: gamma spectra ($CH_2$ + C) of $^{104}$Sn in coincidence with the peak at 1260 keV and with an adjacent gamma energy window.

$^{20}$O [29], $^{44}$Ca [30] and $^{94}$Zr [31] is of the same order of magnitude of the cross section to the $2^+_1$ state ($\sigma_{3^-}/\sigma_{2^+} = 0.5$–1). We therefore propose a spin-parity assignment of $3^-_1$ for the state at 3210 keV, consistent with the systematics of $3^-_1$ excitation energies in stable tin isotopes [28]. The state at 2300 keV is weakly populated so its feeding contribution is negligible. Nevertheless, it was clearly observed in coincidence with the 1260 keV transition and therefore assigned to a $2^+_2$ state on the basis of systematics of heavier tin isotopes. The measured cross sections for $^{104}$Sn inelastic scattering on H are 5.4(24), 4.2(8)($^{+0}_{-10}$), 1.7(9) and 3.9(14)($^{+10}_{-0}$) mb for $2^+_1$, $4^+_1$, $2^+_2$ and the proposed $3^-_1$ states, respectively. The systematic error of 1 mb accounts for the possibility that the 3210 keV state feeds the $4^+_1$ state via a 1280 keV transition that we cannot completely rule out due to the proximity with the strong 1260 keV transition. The cross sections on the C target for the same states are 18.6(41), 3.5(13), 0.88(155) and 5.0(27) mb. If one believes the proposed $3^-_1$ spin-parity assignment of the 3210 keV state, this state lies higher energy with respect to the $3^-_1$ states measured for $A \geq 110$. Its excitation energy of 3210 keV is in good agreement with the prediction of [18].

Fig. 3 shows $2^+$ and $3^-$ experimental excitation energies compared to theoretical values. The latter are obtained from consistent Hartree–Fock–Bogoliubov + QRPA calculations [32] using the Gogny D1M interaction [33]. The Gogny D1M interaction parameters are fitted to all measured masses, with the constraints to provide reliable nuclear matter and neutron matter properties and also radii, giant resonance and fission properties for a selected set of nuclei. The excitation energy of $2^+_1$ states is correctly reproduced. The calculated $3^-_1$ excitation energies overestimate the experimental values by a roughly constant factor. This remains valid for our $^{104}$Sn measurement, if one believes the proposed spin-parity assignment. Thus both experimental and theoretical values would suggest a $3^-_1$ excitation energy rise towards $^{100}$Sn.

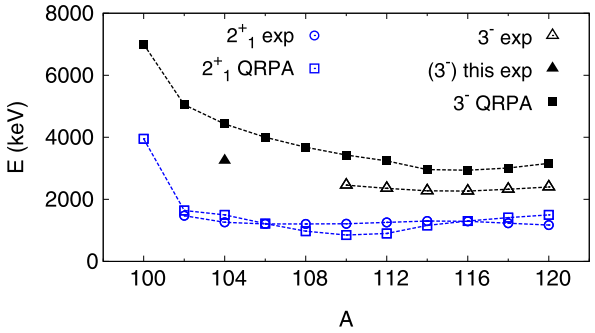


**Fig. 3.** (Color online.) Systematics of $2^+$ and $3^-$ excitation energies in tin isotopes from experiment and HFB + QRPA calculations using the Gogny D1M interaction.

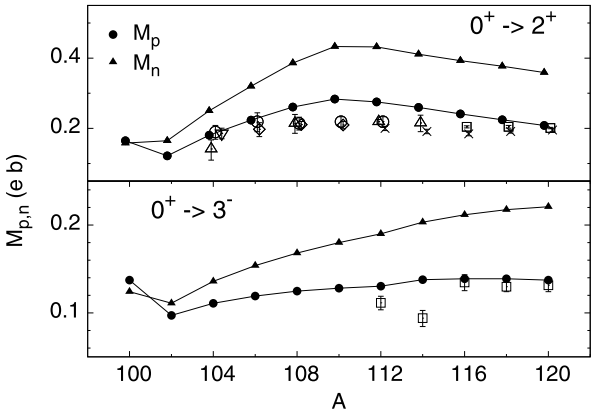


**Fig. 4.** $M_p$ (•) and $M_n$ (▲) from QRPA calculations with the Gogny D1M interaction compared to experimental $M_p$ (▽: RIKEN [14], ○: NSCL [9,13], ×: GSI Doppler Shift Attenuation Method [34], △: GSI Coulomb excitation [6,10–12], ◇: ISOLDE [7,8], □: NNDC [28]). Top: $2^+_1$. Bottom: $3^-_1$. Experimental $M_n$ values are taken from the literature [22].

$M_p$ and $M_n$ of the transitions from the ground state to the $2^+_1$ and $3^-_1$ states obtained within this same theoretical framework are shown in Fig. 4. Both $M_p$ and $M_n$ to the $2^+_1$ state display a maximum of collectivity at $^{110}$Sn and a minimum at $^{102}$Sn, while experimental data show a rather flat dependence on mass between $^{106}$Sn and $^{122}$Sn. An increase of collectivity with decreasing mass until $^{106}$Sn was already predicted by relativistic QRPA calculations [17]. We note that D1M QRPA $M_p$'s to the $2^+_1$ of $^{104,106}$Sn are in agreement with recent measured values [14,9]. $M_p$ and $M_n$ to the $3^-_1$ state decrease linearly from $A = 120$ to $A = 102$. This loss of collectivity is consistent with the high $3^-_1$ state excitation energy in $^{104}$Sn measured in this experiment. This calculation shows that neutron collectivity is the dominant contribution to the $2^+_1$ and $3^-_1$ configurations, as expected in proton-magic isotopes. More importantly, these $M_p$ and $M_n$ values show that the trend of proton collectivity follows the neutron one, except for the doubly magic nucleus $^{100}$Sn. The maximum of collectivity predicted at $A = 110$ and the drop at $A = 102$ indicate that the proton configuration is influenced by neutron excitations. Such a change in both proton and neutron collectivity from $^{112}$Sn to $^{104}$Sn appears in our measured inelastic cross section in conjunction with the B(E2): the $2^+_1$ inelastic excitation cross section decreases by 40(24)% from 9.1(38) mb ($^{112}$Sn) to 5.4(24) mb ($^{104}$Sn), while the B(E2) value evolves by 26(12)% from 0.240(14) $e^2b^2$ to 0.176(22) $e^2b^2$ [13,14].

In order to give credit to this interpretation, we calculated (p, p′) inelastic cross sections within a parameter free approach.

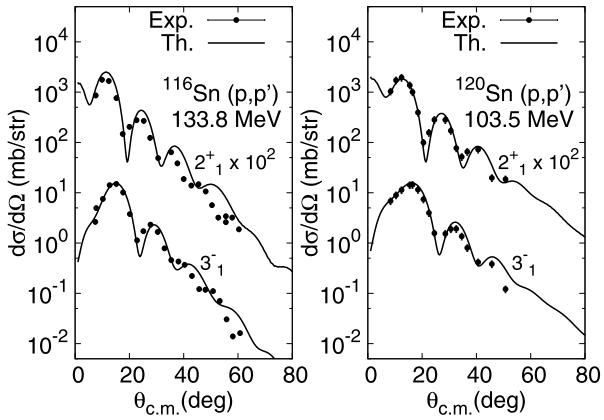


**Fig. 5.** Differential proton inelastic cross sections. Calculated cross sections from the JLM convolution model (full curves) are compared to experimental data (symbols) for the incident energy 133.8 MeV for $^{116}$Sn [37] and 103.5 MeV for $^{120}$Sn [38].

This formalism uses one body neutron and proton local transition densities from QRPA and the semi-microscopic JLM potential [35]. The JLM potential is well suited for inelastic scattering on spherical and near-spherical nuclei with mass $40 < A < 209$ at energies up to 200 MeV/u [36]. First, to estimate the uncertainty related to calculated inelastic cross sections, we compare theoretical and experimental differential cross sections for $^{116,120}$Sn for the first $2^+$ and $3^-$ states. As seen from Fig. 5, predicted angular distribution shapes and magnitudes are in good agreement with measurements without using any normalization factor. We roughly estimate that this agreement is typically within 20%.

Even though $M_n$ values are routinely extracted from such studies, we choose here to discuss only cross sections since only these are observables. Our choice is motivated by the difficulty to assess uncertainties from reaction models. We therefore acknowledge that the following discussion, even though benchmarked on stable nuclei data and performed with care, depends on the details of the chosen reaction model.

Angle integrated calculated cross sections are then compared to the experimental data from this work in Table 1. A good agreement is observed for the population of the $2^+_1$ and $3^-_1$ states both for the $^{112}$Sn benchmark and the $^{104}$Sn case. This consistency gives significant credit to (i) the decrease by a factor $\sim$2 of $M_n$ for the $0^+ \rightarrow 2^+$ transition going from the stable $^{112}$Sn to $^{104}$Sn and (ii) the predominance of $M_n$ over $M_p$ for all Sn isotopes from stability to $^{102}$Sn predicted by QRPA calculations. Note that the second conclusion differs from [14] where the nuclear contribution was roughly estimated from a macroscopic model as a correction to the Coulomb scattering cross section.

One may argue that the calculated $M_p$ values are different from the measured ones for some tin isotopes (e.g. $^{112}$Sn) and such an effect may impact our conclusions. We therefore performed additional cross section calculations only for $^{112}$Sn (since for $^{104}$Sn the measured and calculated $M_p$ coincide) by keeping fixed the theoretical $M_n$ and renormalizing $M_p$ to the experimental value. This yields 5.8(12) and 3.4(7) mb for the cross section to the $2^+_1$ and the tentatively assigned $3^-_1$ state, respectively. The effect is sizable but conclusions are conserved: the decrease of the inelastic cross section is still predicted in agreement with the strong $M_n$ reduction. Indeed, a simple relation exists between the inelastic scattering cross section $\sigma_{inel}$ and $M_{n,p}$:

$$\sigma_{inel} \propto (b_n \times M_n + b_p \times M_p)^2 \quad (1)$$

where $b_{n,p}$ are the neutron and proton field strengths [20].

In the present work, the ratio of inelastic cross sections to the $2^+$ of $^{112}$Sn and $^{104}$Sn is 1.7(10), while the ratio of theoretical estimates is 2.0(6). The strengths of proton and neutron fields are known to be proportional, with a factor that depends on the kind of probe and the beam energy [21]. We have calculated this value for several beam energies and found that the factor $b_n/b_p$ is 2.0–2.5 at beam energy of $\sim$ 130 MeV/u, while it approaches 3 at lower beam energies (10–50 MeV/u), in agreement with experimental findings [21]. Therefore, relation (1) can then be approximated by $\sigma_{inel} \sim b_p^2 \times (2.25 \times M_n + M_p)^2$. If we use this simple relation, we expect a reduction of the cross section to the $2^+$ state by a factor 2.8(7) going from $^{112}$Sn to $^{104}$Sn. Within the error bars, the ratios are still consistent confirming the robustness of the information extracted from inelastic scattering cross sections.

**Table 1**
Gamma-transition energies and extracted inelastic scattering cross sections for excited states in $^{112}$Sn and $^{104}$Sn. Spin-parities displayed between parentheses are those suggested by the present analysis. Theoretical cross sections from QRPA calculations with the Gogny D1M interaction are shown for comparison.

| $^{112}$Sn on H | | | | |
|---|---|---|---|---|
| $J^\pi$ | $E_{ex}$ (keV) | $E_\gamma$ (keV) | $\sigma_{exp}$ (mb) | $\sigma_{th}$ (mb) |
| $2^+_1$ | 1245 | 1245(15) | 9.1(38) | 6.5(13) |
| $0^+_2$ | 2175 | 930(30) | 4.0(24) | $< 0.1$ |
| $4^+_1$ | 2230 | 985(30) | 3.6(26) | 1.8(4) |
| $3^-_1$ | 2335 | 1090(30) | 4.6(20) | 3.6(7) |
| $^{104}$Sn on H | | | | |
| $J^\pi$ | $E_{ex}$ (keV) | $E_\gamma$ (keV) | $\sigma_{exp}$ (mb) | $\sigma_{th}$ (mb) |
| $2^+_1$ | 1260 | 1260(15) | 5.4(24) | 3.2(6) |
| $4^+_1$ | 1930 | 670(20) | $4.2(8)(^{0}_{-10})$ | 0.7(1) |
| $(2^+_2)$ | 2300 | 1040(20) | 1.8(9) | 0.3(1) |
| $(3^-_1)$ | 3210 | 1950(50) | $3.8(14)(^{+10}_{0})$ | 3.0(6) |

In summary, we measured the inclusive proton-induced inelastic scattering of low lying states in $^{104}$Sn, the first measurement of this kind in a light tin isotope. We performed a similar measurement with $^{112}$Sn as a benchmark. We tentatively identify the transition at 1950(50) keV in $^{104}$Sn with the decay of a $3^-$ state at 3210(50) keV, the first one observed in neutron deficient tin isotopes. The measurement is at the limits of feasibility, due to the low, although most intense worldwide, $^{104}$Sn beam intensity. We have performed QRPA calculations with the Gogny D1M interaction and adopted them as input for the cross section calculation using the JLM convolution model. The QRPA calculations display a dominance of neutron over proton collectivity, with $M_n/M_p = 1.4$ and 1.6 for $^{104,112}$Sn($2^+$). We have observed a reduction in the population of the $2^+_1$ state from $^{112}$Sn to $^{104}$Sn, in agreement with predictions. This gives credit to the interpretation of a strong neutron collectivity ($M_n$) reduction from $^{112}$Sn to $^{104}$Sn. The predicted isoscalar excitation of protons and neutrons suggests that the $M_p$ ($L = 2$) plateau observed from stable tin isotopes to $^{106}$Sn is induced by an increased neutron collectivity.

## Acknowledgements

This work has been supported by the European Research Council through the ERC Starting Grant No. MINOS-258567 and by the ENSAR European FP7 Project No. 262010. A. Jungclaus acknowledges support from the Spanish Ministerio de Ciencia e Innovacion under Contracts No. FPA2009-13377-C02-02 and No. FPA2011-29854-C04-01. D. Sohler acknowledges travel support from Hungarian Scientific Research funds (Contracts No. K100835 and No. NN104543).

## References

[1] T. Motobayashi, et al., Phys. Lett. B 346 (1995) 9.
[2] B. Bastin, et al., Phys. Rev. Lett. 99 (2007) 022503.

[3] A. Obertelli, et al., Phys. Lett. B 633 (2006) 33.
[4] C.B. Hinke, et al., Nature 486 (2012) 341.
[5] K.L. Jones, et al., Nature 465 (2010) 454.
[6] A. Banu, et al., Phys. Rev. C 72 (2005) 061305.
[7] A. Ekström, et al., Phys. Rev. Lett. 101 (2008) 012502.
[8] J. Cederkäll, et al., Phys. Rev. Lett. 98 (2007) 172501.
[9] C. Vaman, et al., Phys. Rev. Lett. 99 (2007) 162501.
[10] P. Doornenbal, et al., Phys. Rev. C 78 (2008) 031303.
[11] R. Kumar, et al., Phys. Rev. C 81 (2010) 024306.
[12] G. Guastalla, et al., Phys. Rev. Lett. 110 (2013) 172501.
[13] V.M. Bader, et al., Phys. Rev. C 88 (2013) 051301.
[14] P. Doornenbal, et al., Phys. Rev. C 90 (2014) 061302.
[15] T. Bäck, et al., Phys. Rev. C 87 (2013) 031306.
[16] A. Ansari, Phys. Lett. B 623 (2005) 37.
[17] A. Ansari, P. Ring, Phys. Rev. C 74 (2006) 054313.
[18] B.G. Carlsson, J. Toivanen, A. Pastore, Phys. Rev. C 86 (2012) 014307.
[19] S. Péru, M. Martini, Eur. Phys. J. A 50 (2014) 88.
[20] A. Bernstein, V. Brown, V. Madsen, Phys. Lett. B 103 (1981) 255.
[21] A. Bernstein, V. Brown, V. Madsen, Comments Nucl. Part. Phys. 11 (1983) 203.
[22] M. Kennedy, P. Cottle, K. Kemper, Phys. Rev. C 46 (1992) 5.
[23] P. Blankert, H. Blok, J. Blok, Nucl. Phys. A 356 (1981) 74.
[24] T. Kubo, et al., Nucl. Instrum. Methods Phys. Res. 2012 (2012).
[25] S. Takeuchi, T. Motobayashi, Y. Togano, M. Matsushita, N. Aoi, K. Demichi, H. Hasegawa, H. Murakami, Nucl. Instrum. Methods A 763 (2014) 596.
[26] L. Audirac, et al., Phys. Rev. C 88 (2013) 041602.
[27] S. Agostinelli, et al., Nucl. Instrum. Methods 506 (2003) 250.
[28] NNDC, www.nndc.bnl.gov.
[29] E. Khan, et al., Phys. Lett. B (ISSN 0370-2693) 490 (2000) 45.
[30] R. Peterson, D. Perlman, Nucl. Phys. A 117 (1968) 185.
[31] J.K. Dickens, E. Eichler, G.R. Satchler, Phys. Rev. 168 (1968) 1355.
[32] S. Péru, H. Goutte, Phys. Rev. C 77 (2008) 044313.
[33] S. Goriely, S. Hilaire, M. Girod, S. Péru, Phys. Rev. Lett. 102 (2009) 242501.
[34] A. Jungclaus, et al., Phys. Lett. B 695 (2011) 110.
[35] E. Bauge, et al., Phys. Rev. C 61 (2000) 034306.
[36] E. Bauge, J.P. Delaroche, M. Girod, Phys. Rev. C 63 (2001) 024607.
[37] S. van der Werf, et al., Phys. Lett. B 166 (1986) 372.
[38] S. Kailas, P.P. Singh, D.L. Friesel, C.C. Foster, P. Schwandt, J. Wiggins, Phys. Rev. C 29 (1984) 2075.